

Supporting Information

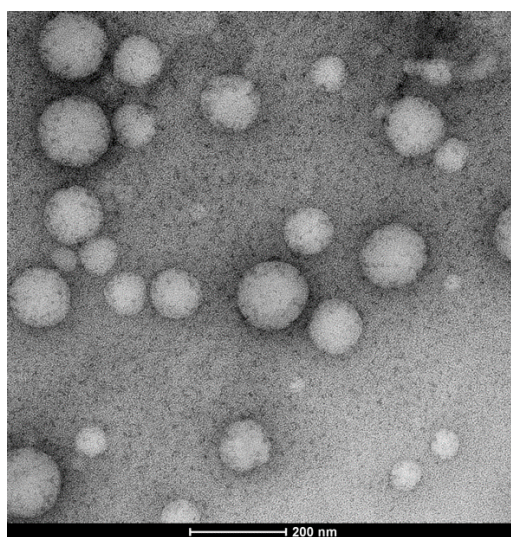
Albumin-polymer conjugate nanoparticles and their interactions with prostate cancer cells in 2D and 3D culture: Degradable vs non-degradable polymers

Yanyan Jiang¹, Hongxu Lu¹, Aydan Dag², Gene Hart-Smith³, Martina H. Stenzel^{1,*}

¹Centre for Advanced Macromolecular Design (CAMD), School of Chemical Engineering and School of Chemistry, University of New South Wales, Sydney, NSW 2052, Australia

² Department of Pharmaceutical Chemistry, Faculty of Pharmacy, Bezmialem Vakif University, 34093 Fatih, Istanbul, Turkey

³Systems Biology Initiative, School of Biotechnology and Biomolecular Sciences, University of New South Wales, Sydney 2052, Australia



Sample name	Hydrodynamic diameter (nm)	PDI
BSA-PMMA nanoparticle	147±11	0.35

Figure S1: TEM image and the DLS information of BSA-PMMA nanoparticles.

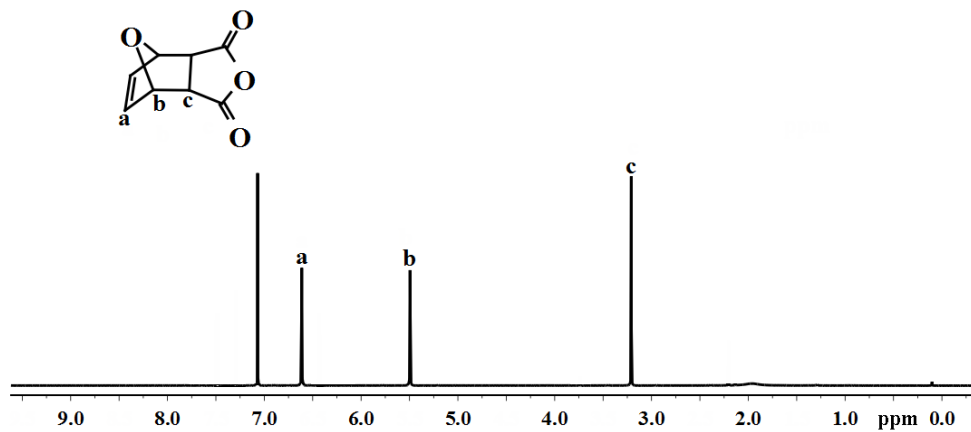


Figure S2: ¹H NMR spectrum of 4,10-dioxatricyclo[5.2.1.0^{2,6}]dec-8-ene-3,5-dione (**1**) in CDCl₃.

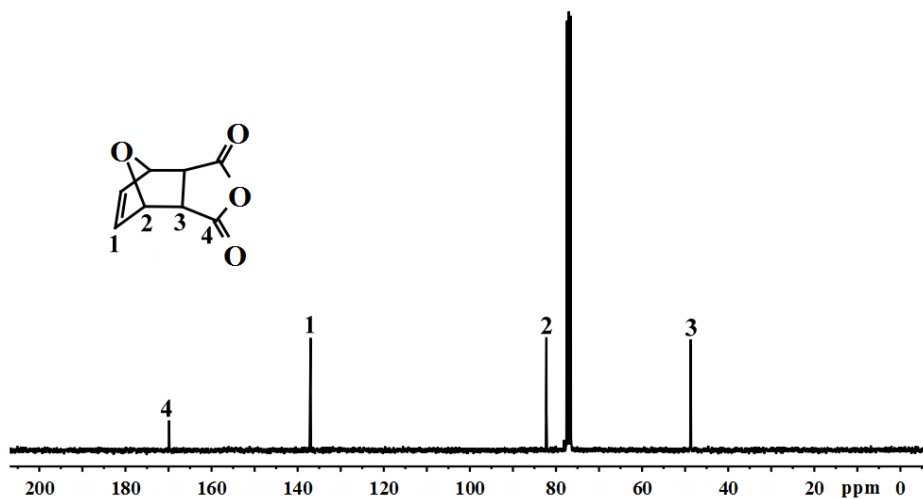


Figure S3: ¹³C NMR spectrum of 4,10-dioxatricyclo[5.2.1.0^{2,6}]dec-8-ene-3,5-dione (**1**) in CDCl₃.

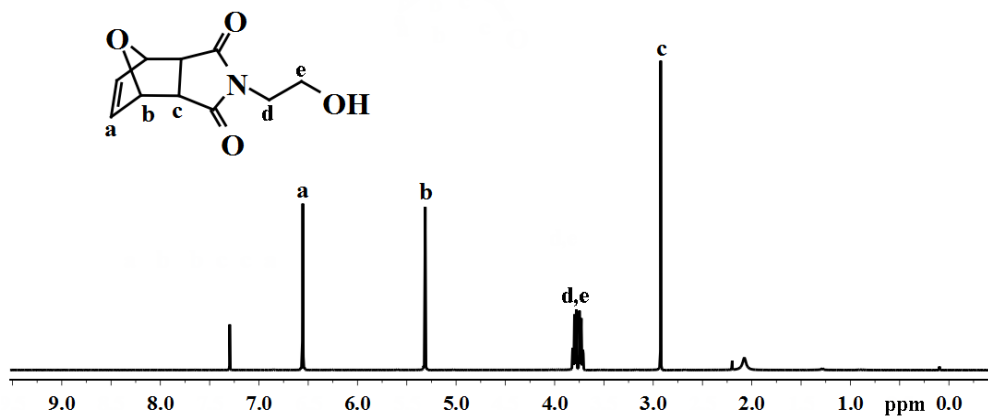


Figure S4: ^1H NMR spectrum of 4-(2-hydroxyethyl)-10-oxa-4-azatricyclo[5.2.1.0^{2,6}]dec-8-ene-3,5-dione (2) in CDCl_3 .

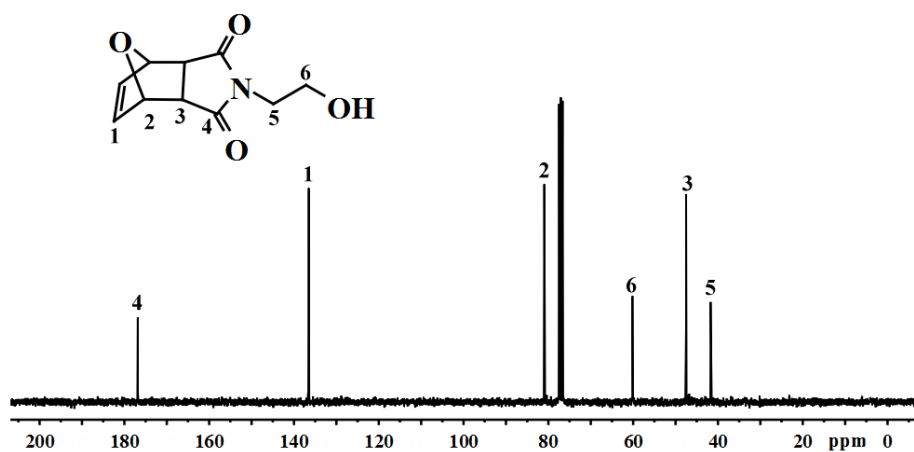


Figure S5: ^{13}C NMR spectrum of 4-(2-hydroxyethyl)-10-oxa-4-azatricyclo[5.2.1.0^{2,6}]dec-8-ene-3,5-dione (2) in CDCl_3 .

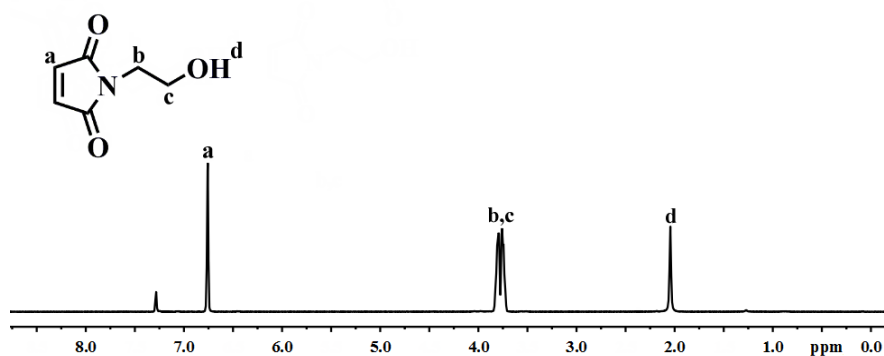


Figure S6: ^1H NMR spectrum of 1-(2-hydroxyethyl)-1H-pyrrole-2,5-dione (3) in CDCl_3 .

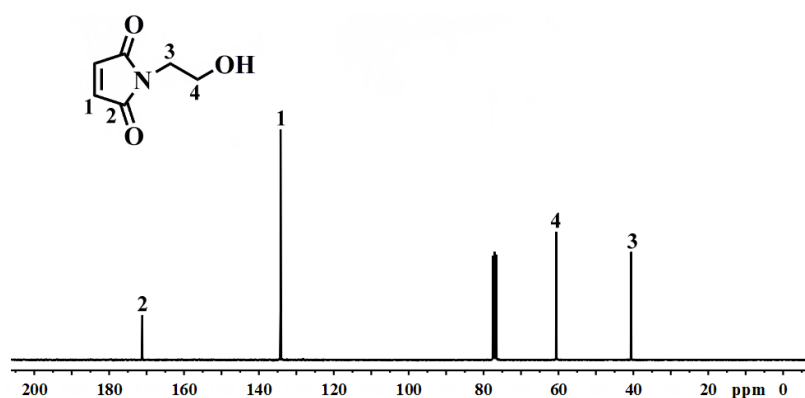


Figure S7: ^{13}C NMR spectrum of 1-(2-hydroxyethyl)-1H-pyrrole-2,5-dione (3) in CDCl_3 .

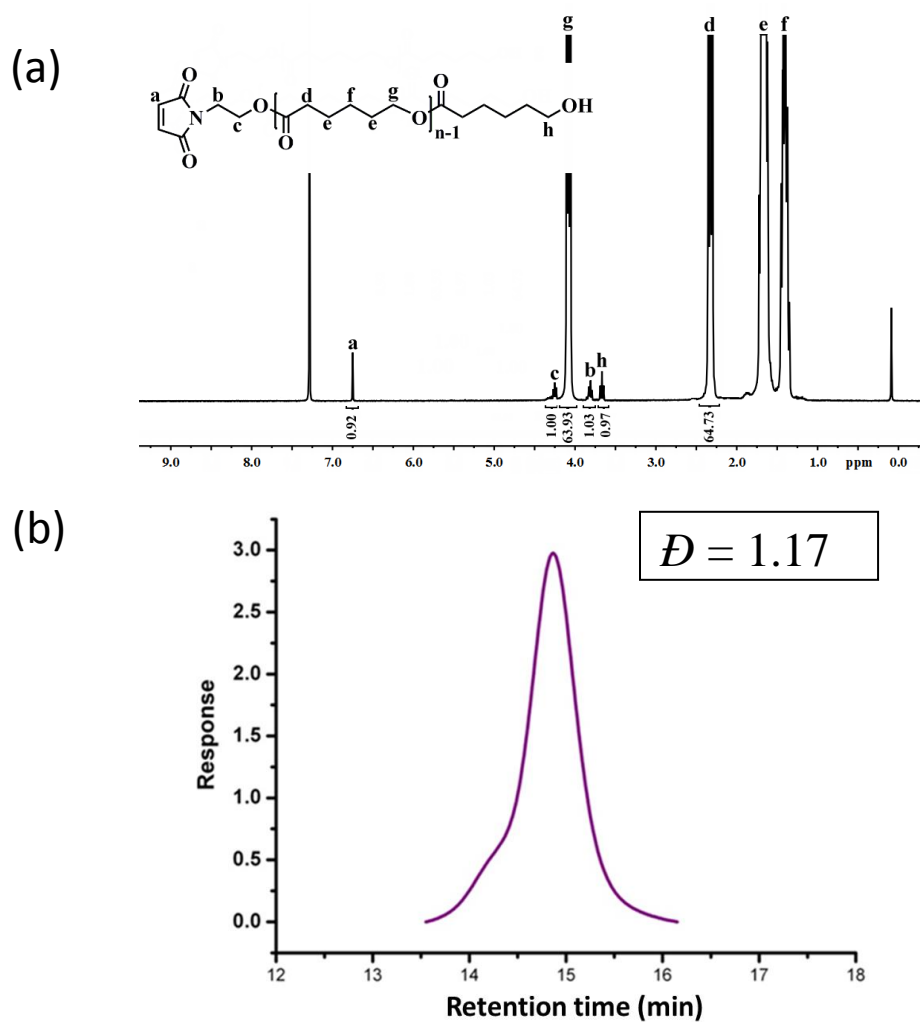


Figure S8: (a) ^1H NMR (CDCl_3) spectra of MI-PCL and (b) GPC curve.

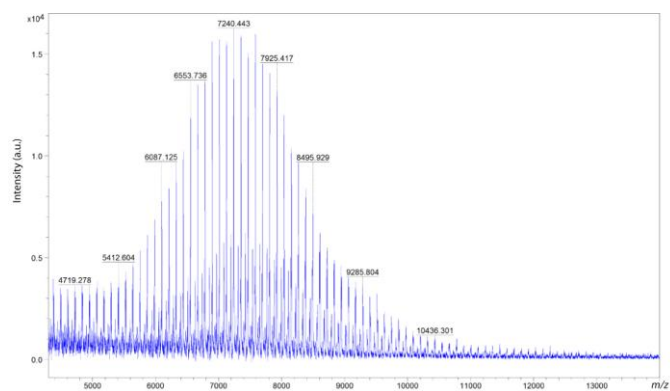


Figure S9: The MALDI-TOF spectrum of PCL. 2,5-Dihydroxybenzoic acid (DHB) (20 mg/mL in 70:30 acetonitrile:0.1% tetrafluoroacetic acid) was used as the matrix.

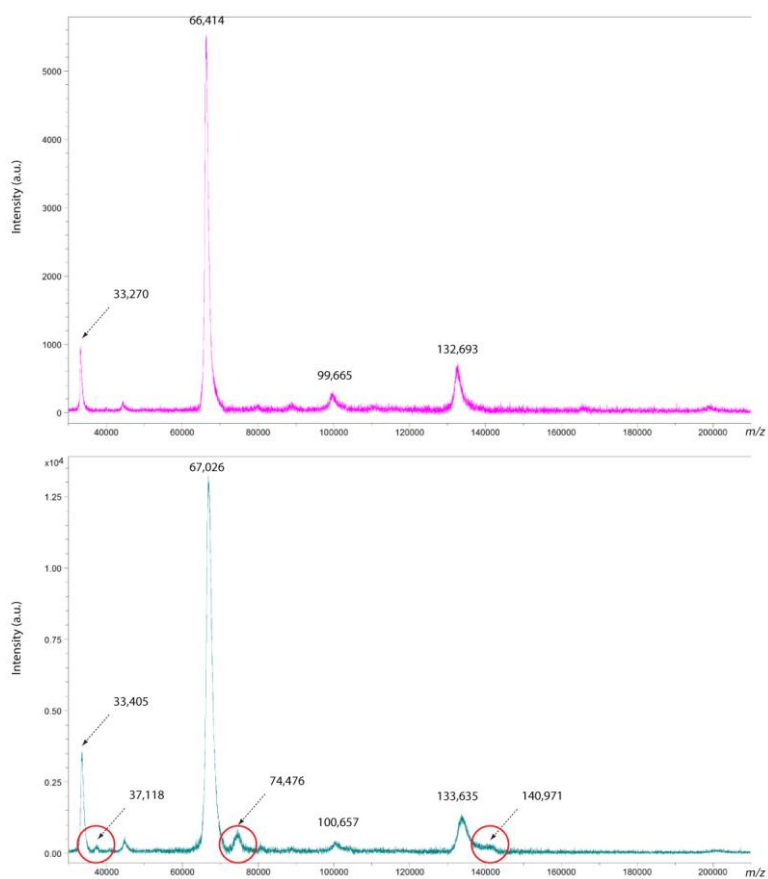


Figure S10: MALDI-TOF spectra of BSA (top) and the BSA-PCL conjugate mixture (bottom). 2,5-Dihydroxybenzoic acid (DHB) (20 mg/mL in 70:30 acetonitrile:0.1% tetrafluoroacetic acid) was used as the matrix. The peaks of the conjugates have been marked with red circles.

Table S1. The particle size of the BSA-PCL micelles with deferent treatment.

Sample Name	Particle size (d. nm)	PDI
BSA-PCL micelle blank	111.23	0.20
BSA-PCL micelle blank 5 days	108.49	0.19
BSA-PCL micelle blank with trypsin	>1000	1
BSA-PCL micelle blank with pancreatin	0	0

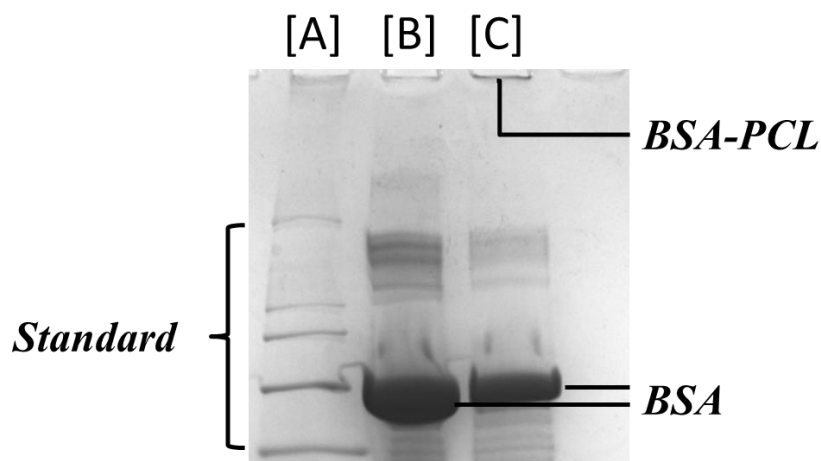


Figure S11: SDS-PAGE traces of the conjugation of BSA and PCL (molar ratio= 1:1). Lane [A]: protein standard. [B]: Initial BSA. [C]: BSA-PCL micelle. The amphiphilicity of the BSA-PCL conjugates prevents the diffusion of the final product, which is only visible in the well. Comparing the intensity of the BSA residual band in Lane [C] with the initial BSA band in Lane [B], around 50 % of BSA has been conjugated to the maleimide PCL.

Table S2. Final concentrations of inhibitors used for the cytotoxicity assay.

Inhibitor	Final concentrations
Chorprozamine hydrochloride	10 µg/mL
Filipin	10 µg/mL
Amiloride	50 µM
NaN₃/Deoxyglucose	5 mM/5 mM

Table S3. Summary of inhibitor targets and mechanisms of action.

Inhibitor	Targeted Pathway	Mechanism of Action
Chlorpromazine	Clathrin	Prevention of coated pit formation
Filipin	Lipid Raft/Caveolae	Binding to cholesterol causing sequestration
Amiloride	Macropinocytosis	Na ⁺ /H ⁺ Exchanger inhibition
NaN₃	Receptor mediated	ATP depletion

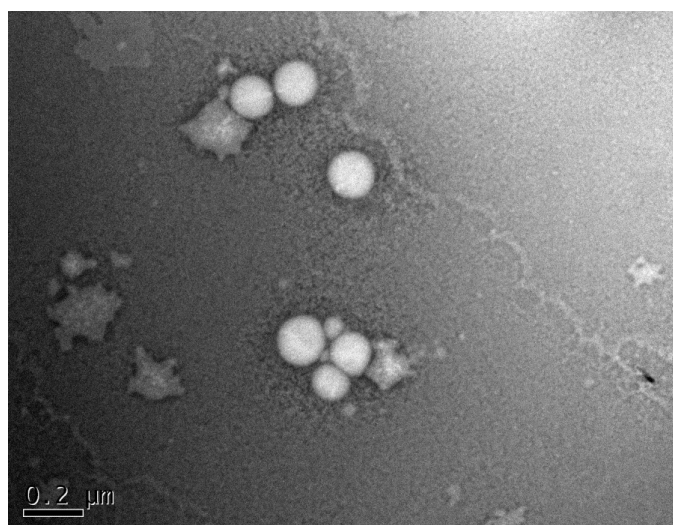


Figure S12: TEM image of the Nile red loaded BSA-PCL micelles.

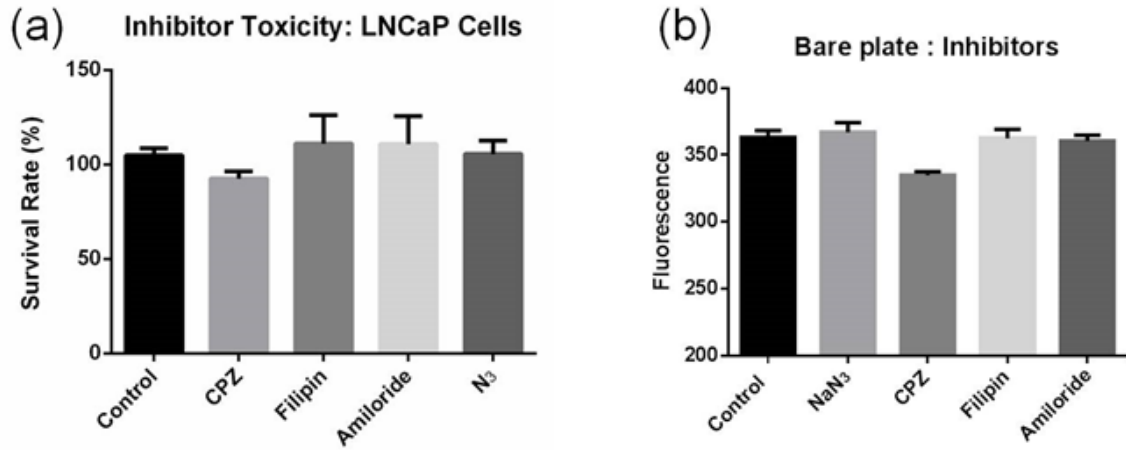


Figure S13: (a) Cytotoxicity test of all the four inhibitors. (b) The influence of the inhibitors on the fluorescence of the BSA-PCL micelle without cells. Data represent means \pm S.D., $n=4$.

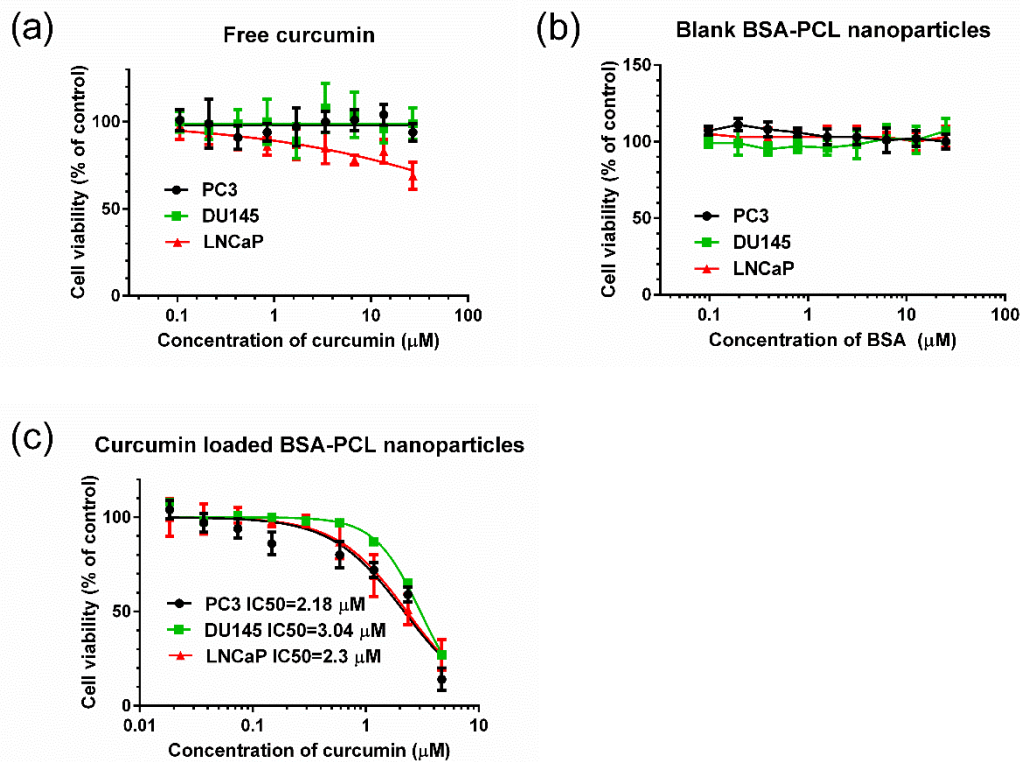


Figure S14. Cytotoxicity assays of (a) free curcumin, (b) blank BSA-PCL nanoparticles and (c) curcumin loaded BSA-PCL nanoparticles against prostate carcinoma cell lines (PC3, DU145 and LNCaP) for 48 h. The mean \pm standard deviations are shown.